THE JOURNAL OF PHYSICAL CHEMISTRY A

pubs.acs.org/JPCA Article

Metal and Ligand Effects on Coordinated Methane pK_a: Direct Correlation with the Methane Activation Barrier

Amy S. Guan, Ivy X. Liang, Christopher X. Zhou, and Thomas R. Cundari*

Cite This: *J. Phys. Chem. A* 2020, 124, 7283–7289 Read Online

ACCESS | Metrics & More | Article Recommendations | Supporting Information

ABSTRACT: DFT and coupled cluster methods were used to investigate the impact of 3d metals and ligands upon the acidity and activation of coordinated methane C−H bonds. A strong, direct relationship was established between the pK_a of coordinated methane and the free energy barriers ($\Delta G^{\ddagger}$) to subsequent H_3C−H activation. The few outliers to this relationship indicated other salient factors (such as thermodynamic stability of the product and ligand−metal coordination type) that impacted the methane activation barrier. High variations in the activation barriers and pK_a values were found with a range of 34.8 kcal/mol for the former and 28.6 pK_a units for the latter. Clear trends among specific metals and ligands were also derived; metal ions such as Co^{I}, as well as Lewis acids and π-acids, consistently yielded higher acidity for ligated methane and hence lower $\Delta G^{\ddagger}$.

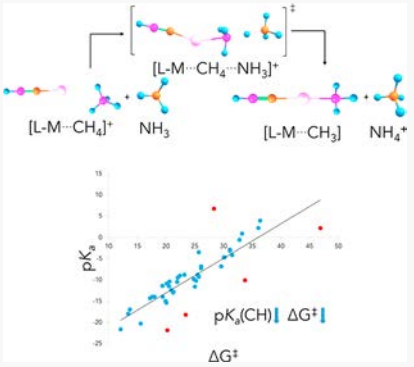

INTRODUCTION

Methane is an abundant hydrocarbon and a major constituent of natural gas.[1] Methanol, a liquid fuel with a wide range of applications, provides a cleaner source of energy than traditional fossil fuels and can act as a chemical feedstock in place of petroleum.[1,2] Furthermore, methanol retains much of the energetic properties of methane and, being a liquid, has the added benefit of being much more efficient to transport.[1,3] Thus, methane functionalization, which can be used to produce methanol, remains a prominent area of study in energy research.[1−3] However, because methane is highly unreactive, the selective conversion of methane to methanol is impractical without the aid of catalysts.[1,2]

A study by Olah and Schlosberg[4] indicated that methane, which is typically a very stable hydrocarbon, is only readily protonated under extreme conditions using superacids. Similarly, a study by Streitwieser and Taylor[5] suggested that methane is an extremely poor Brønsted−Lowry acid, except in the presence of superbases. However, superacidic and superbasic solutions involve impractical, extreme conditions, and highly reactive reagents that are typically characterized by stoichiometric rather than catalytic reactivity. Transition metal catalysis poses an alternative catalytic approach to methane functionalization that occurs under milder conditions and with higher selectivity.[2,6]

One method to increase the favorability of methane activation involves studying how various transition metals and supporting ligands impact the pK_a of a ligated methane C−H bond and hence facilitate its eventual activation.[7,8] Previous studies have shown the significance of pK_a in promoting bond activation. In the field of biocatalysis, Pitsawong et al.[7] investigated the use of flavin-dependent mono-oxygenases to catalyze phenol oxidation. Their study found that the binding of the mono-oxygenase to the phenol reduced its acidity by 1.6−2.5 pK_a units, based on protein type, thus enhancing the catalysis. These results highlight the importance of substrate acid/base properties in biocatalysis. The challenge for methane activation is a much more drastic requirement for pK_a reduction of its C−H bond prior to activation. In a rare computational study of the pK_a(C−H) of methane coordinated to "naked", monovalent 3d metal ions by Zhou and Cundari,[8] it was demonstrated that the metal ion has a substantial impact on increasing the C−H bond acidity of methane; metal identity provided a significant difference in calculated ΔpK_a(C−H) ranging from 8 to 36 pK_a units.

While previous reports have focused on the pK_a(C−H) of organic acids,[9] studies on the pK_a of C−H bonds in hydrocarbons that are coordinated to metals are rare.[8] This area of chemistry has been understudied largely due to the traditional experimental limitations of measuring pK_a for very weak hydrocarbon acids, despite the importance of pK_a in determining catalytic potential.[10] Furthermore, little is known about the possible correlation of pK_a(C−H) with C−H activation barriers. As a result, this computational study was initiated.

Received: May 26, 2020
Revised: August 4, 2020
Published: August 10, 2020

https://dx.doi.org/10.1021/acs.jpca.0c04756
J. Phys. Chem. A 2020, 124, 7283−7289

Building off the conclusions derived from the study by Zhou and Cundari,[8] this research examined the coordination of methane to complexes composed of 3d metals (M = Fe^{I}, Co^{I}, Ni^{I}, Cu^{I}) and coordinated neutral supporting ligands (L = AlH_3, BH_3, HNC, CO, HCN, H_2O, NH_3, PH_3, SH_2) of differing donor/acceptor properties. Theory was used to determine the effect of metal and ligand identity on the acidity of coordinated methane, and the subsequent favorability of methane deprotonation. A Brønsted−Lowry acid−base reaction was investigated for methane activation. The reaction involved a transition metal−methane adduct of the form $[L{-}M{\cdots}CH_4]^+$ (Figure 1)

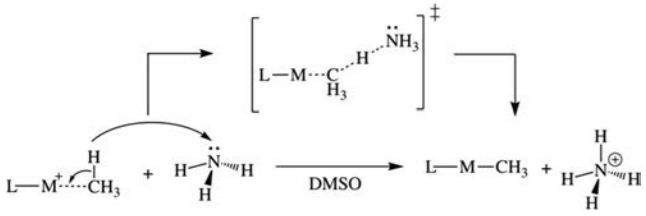

Figure 1. Acid−base reaction used to obtain the free energy barriers, free energy changes, and pK_a values relevant to methane activation: a cationic ligand−metal methane adduct and an ammonia molecule, in SMD-DMSO (SMD = solvent model density) continuum solvent, react, which results in a ligand−metal−methyl complex and an ammonium ion.

reacting with the Lewis base NH_3 in a continuum solvent dimethyl sulfoxide (DMSO). All 3d metal ions were assumed to have a formal oxidation state of 1+ to facilitate comparisons among them. Likewise, all studied ligands are formally neutral. In the reaction of interest, Figure 1, methane is loosely coordinated to the metal of the LM^+ complex. During the transition state (TS), a formal proton transfer occurs, activating the methane and producing ammonium. As the reaction proceeds to completion, the bond between the methane and the metal ion is strengthened by the transfer of electrons from the C−H bond to the metal−methyl bond. Thus, a neutral methyl complex $[L{-}M{-}CH_3]$ is produced, as the conjugate base of the cationic methane adduct.

Methodology. All geometries in this study were optimized at the B3LYP/6-31+G(d)/SMD-DMSO level of theory within the *Gaussian16*[11] software package. Vibrational frequencies were computed to ensure the appropriate number of imaginary frequencies, as well as obtain the enthalpic and entropic corrections needed for free energy calculations. Single-point energies were calculated at the optimized geometries using the ORCA code (version 4.2.1),[12,13] by employing the DLPNO-CCSD(T) technique in conjunction with the def2-QZVPP basis set. The basis set choice was derived from a previous report,[8] which indicated that quadruple-ζ basis sets provided an accuracy comparable to that of quintuple-ζ basis sets with lower expense. Their methodology, as in the present research, utilized the SMD continuum solvent model to simulate a DMSO solution. Additionally, the T_1 diagnostic was used to assess the reliability of the CCSD(T) calculations. All T_1 values were below the threshold of 0.15, with the majority of T_1 values below 0.05, excluding a few exceptions for Mn complexes, which will be revisited later.

For the modeled reaction of the form $[L{-}M{\cdots}CH_4]^+ + NH_3 \rightarrow [L{-}M{-}CH_3] + NH_4^+$, Figures 1 and 2, data consisting of the single-point energy and DFT-computed thermal correction to the Gibbs free energy for the reactants, transition state, and

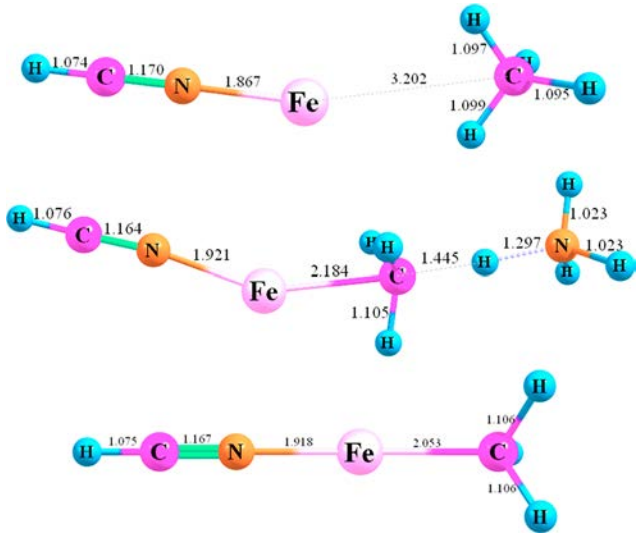

Figure 2. B3LYP/6-31+G(d)/SMD-DMSO-optimized HCN−Fe^+ complexes (HCN−Fe^I−methane adduct, top; HCN−Fe^I transition state for methane activation by ammonia, middle; the conjugate base, HCN−Fe^I−methyl complex, bottom) as representative examples of geometries obtained for stationary points modeled in this study. Bond lengths in Å.

products were used to compute the pK_a, Gibbs free energy of deprotonation (ΔG), and Gibbs free energy barrier ($\Delta G^{\ddagger}$, methane activation barrier) for each reaction. Initial pK_a values were computed using the following equation: $pK_a\text{calc} = \frac{\Delta G}{2.303RT}$. Then, the following linear correction derived from the work of Nazemi and Cundari[14] was applied to the calculated pK_a value

$$pK_a\text{est} = (1.0308pK_a\text{calc}) - 12.146$$

to obtain the final estimated pK_a(C−H) of the methane adduct, $[L{-}M{\cdots}CH_4]^+$.

The GEI (global electrophilicity index) was calculated as a metric for Lewis acidity.[15] First, μ, the chemical potential, was computed using the equation $\mu = \frac{1}{2}(E_{HOMO} + E_{LUMO})$, and η, the chemical hardness, was computed thusly, $\eta = E_{LUMO} - E_{HOMO}$. Next, ω, the GEI in eV, was computed using the following equation

$$\omega = \frac{27.212\mu^2}{2\eta}$$

to obtain the Lewis acidity of each ligand investigated.

RESULTS AND DISCUSSION

The predicted ground state multiplicities of the ligand−3d metal methane adducts (Table S-1) agreed with the lowest energy multiplicities proposed in a study that modeled methane adducts of 3d ions in the absence of any supporting ligands.[8] One exception was the Fe^I ion, where DLPNO-CCSD(T)/def2-QZVPP/SMD-DMSO (hereafter CCSD(T)) calculations predicted a quartet ground state for all $[LFe^+{\cdots}CH_4]$, whereas Zhou and Cundari[8] predicted a sextet ground state for $[Fe^+{\cdots}CH_4]$. While the quartet was consistently shown to provide a lower energy ground state, the difference in energy between the quartet and sextet states was small, with the former being lower by only a few kcal/mol. The CCSD(T) calculations indicated that the quartet state was more favorable for the Fe^I methane adducts. A second caveat was the case of the Mn^I ion, where

https://dx.doi.org/10.1021/acs.jpca.0c04756
J. Phys. Chem. A 2020, 124, 7283−7289

CCSD(T) calculations predicted a combination of quintet and septet ground states for $[LMn^{+}\cdots CH_4]$ while Zhou and Cundari[8] predicted a septet ground state for naked Mn^{I} ion complexes. This possible discrepancy is similar to that of Fe^{I} in which certain ground spin states predicted by DFT and CCSD(T) did not align. Finally, no correlation was found between spin state and free energy barrier (see Figures S-1 and S-2).

In Tables 1 and 2, using the DLPNO-CCSD(T)/def2-QZVPP/SMD-DMSO//B3LYP/6-31+G(d)/SMD-DMSO level of theory, the free energy barriers for methane activation and the estimated pK_a(C−H) values were computed and are displayed for each ligand−metal pair. The corresponding free energies for the overall reaction from which pK_a(C−H) values were derived are summarized in Supporting Information. Figures 3 and 4 show the free energy barriers computed for the different L/M combinations studied.

Table 1. Free Energy Barriers (kcal/mol) for Methane Activation by Ammonia for 3d $[LM\cdots CH_4]^{+}$ Adducts[a]

L	Mn^{I}	Fe^{I}	Co^{I}	Ni^{I}	Cu^{I}
AlH_3	20.2	24.7	12.1	28.7	23.4
BH_3	15.6	18.0	17.6	24.8	33.7
HNC	21.2	22.4	20.5	30.2	21.9
CO	19.4	17.2	13.7	25.7	19.9
HCN	20.0	21.3	20.1	31.1	20.9
NH_3	36.4	32.8	26.1	36.1	26.1
H_2O	28.2	29.6	22.0	31.1	25.0
PH_3	46.9	25.5	20.6	31.5	25.6
SH_2	33.2	25.7	23.2	30.1	25.2

[a]Computed at the DLPNO-CCSD(T)/def2-QZVPP/SMD-DMSO//B3LYP/6-31+G(d)/SMD-DMSO Level of Theory.

Table 2. Estimated pK_a Values of Ligand−3d Metal Methane Adducts Computed from the ΔG Values in Table S-2[a]

L	Mn^{I}	Fe^{I}	Co^{I}	Ni^{I}	Cu^{I}
AlH_3	−21.8	−9.5	−21.6	−6.9	−18.2
BH_3	−20.3	−14.0	−14.0	−10.3	−10.1
HNC	−13.0	−9.0	−11.5	−4.7	−10.5
CO	−11.4	−14.3	−17.0	−9.3	−15.0
HCN	−15.4	−12.8	−10.9	−2.9	−12.4
NH_3	3.9	−0.6	−6.8	2.2	−7.3
H_2O	6.8	−6.8	−9.5	−3.2	−11.6
PH_3	2.2	−8.8	−10.4	−4.2	−9.1
SH_2	0.9	−3.5	−8.8	−4.7	−10.2

[a]Calculated at the DLPNO-CCSD(T)/def2-QZVPP/SMD-DMSO//B3LYP/6-31+G(d)/SMD-DMSO level of theory.

In general, lower free energy barriers were calculated for the Lewis acids, AlH_3 and BH_3, and the π-acid CO. The highest $\Delta G^{\ddagger}$ values were obtained for Lewis bases such as $NH_3$and H_2O with the exception of Mn-PH_3, Figure 3. On the other hand, the lowest free energy barrier values obtained alternated between the Lewis acids AlH_3 and BH_3 and the π-acid CO. In terms of pK_a, AlH_3 provided the lowest pK_a values for each of the metals, except for Fe and Ni, modeled herein, Figure 5.

The LCo^{I} complexes consistently provided the lowest methane activation barrier for each ligand among all five metals tested except in the case of BH_3−Mn^{I}, Figure 4. Thus, the LCo^{I} complexes yielded the lowest average free energy barrier of 19.5 ± 4.4 kcal/mol among all five metals tested, Table 4. However, despite this generally strong consistency, LCo^{I} complexes did not always result in the lowest pK_a value for each ligand among the other LM^{+} complexes, Figure 6. The LNi^{I} complexes generally had the highest methane activation barriers and pK_a values except when compared to some of the Lewis base ligand pairings with Mn^{I}, Figures 4 and 6. Additionally, Mn^{I} was an unusual case in that the curves for LMn^{I} did not always conform

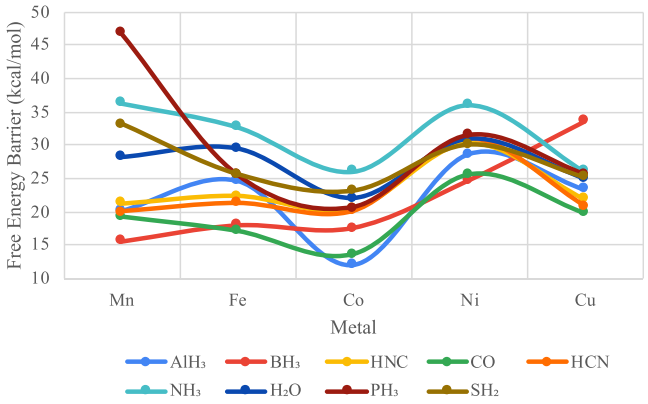

Figure 3. DLPNO-CCSD(T)/def2-QZVPP/SMD-DMSO//B3LYP/6-31+G(d)/SMD-DMSO calculated free energy barriers (kcal/mol) for methane activation for the various ligand−metal complexes organized by metal.

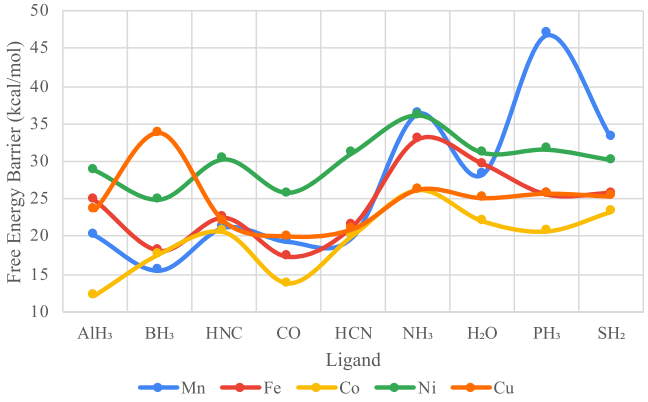

Figure 4. DLPNO-CCSD(T)/def2-QZVPP/SMD-DMSO//B3LYP/6-31+G(d)/SMD-DMSO calculated free energy barriers (kcal/mol) for methane activation among the ligand−metal complexes organized by ligand.

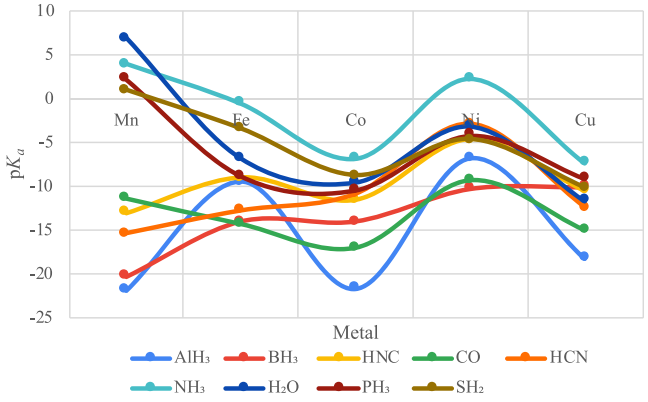

Figure 5. DLPNO-CCSD(T)/def2-QZVPP/SMD-DMSO//B3LYP/6-31+G(d)/SMD-DMSO calculated pK_a(C−H) trends for the various ligand−metal methane adducts organized by metal.

https://dx.doi.org/10.1021/acs.jpca.0c04756
J. Phys. Chem. A 2020, 124, 7283−7289

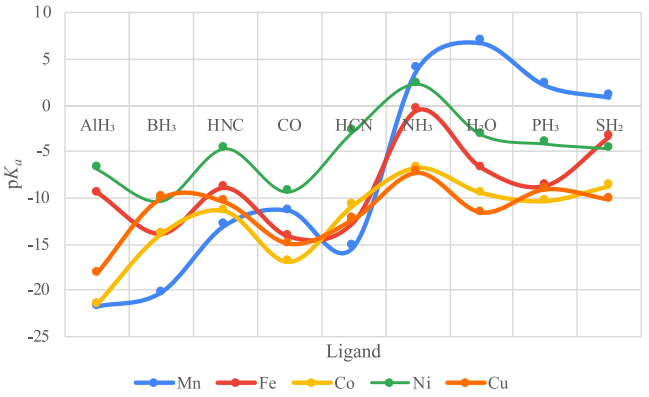

Figure 6. DLPNO-CCSD(T)/def2-QZVPP/SMD-DMSO//B3LYP/6-31+G(d)/SMD-DMSO calculated pK_a(C−H) trends among the various ligand−metal methane adducts organized by ligand.

to the trends seen across the other four metals, Figures 4 and 6, a point we revisit below.

Table 3 organizes the average and standard deviations for the $\Delta G^{\ddagger}$ and the estimated pK_a values for the ligand−3d metal methane adducts by ligand. Table 4 organizes the same averages and standard deviations by metal. The results indicated that LCo^{I} yielded the lowest average $\Delta G^{\ddagger}$ of 19.5 kcal/mol and lowest average methane pK_a of −12.3 pK_a units. LCu^{I} yielded the second lowest standard deviation in calculated $\Delta G^{\ddagger}$, ±4.0 kcal/mol, and pK_a, ±3.3 pK_a units. Hence, the results suggest that the d^{10}-CuL^{+} complexes showed the least sensitivity to ligand modification; it is hypothesized that this may be a reflection of the closed-shell nature of the Cu^{I} ion. Additionally, the standard deviations for LMn^{I} complexes were significantly higher than those found for other metal complexes. A contributing factor for this and its unusual trends in Figures 4 and 6 may be the T_1 diagnostic values found for the complexes of the quintet spin state for Mn^{I}, whose values were occasionally >0.15, suggesting possible issues with their DLPNO-CCSD(T) description. Next, the results indicated that CO yielded the lowest average $\Delta G^{\ddagger}$ of 19.2 kcal/mol, while AlH_3 yielded the lowest average pK_a of −15.6 pK_a units. The H_2O ligand yielded the smallest standard deviation in $\Delta G^{\ddagger}$, ±3.7 kcal/mol, and the CO ligand yielded the smallest standard deviation in pK_a, ±3.0 pK_a units. Upon closer observation, these data suggest a correlation between pK_a(C−H) values for the ligated methane and its subsequent activation barrier.

Figure 7 indicates that the free energy barrier of the methane deprotonation and the pK_a of the reaction have a positive, linear correlation (R^2 = 0.70 with outliers included). Five outliers were found: AlH_3−Cu^{I}, BH_3−Cu^{I}, AlH_3−Cu^{I}, H_2O−Mn^{I}, and PH_3−Mn^{I}, all denoted by red dots in Figure 7. All of the outliers involved copper or manganese among the metals, and the majority involved Lewis acid supporting ligands, AlH_3 or BH_3.

Table 4. Average and Standard Deviations of Calculated Properties (Free Energy Barriers (kcal/mol) and pK_a (pK_a Units)) of Ligand−3d Metal Adducts for Each Metal[a]

	Mn^{I}	Fe^{I}	Co^{I}	Ni^{I}	Cu^{I}
$\Delta G^{\ddagger}$ ave	26.8	24.1	19.5	29.9	24.6
$\Delta G^{\ddagger}$ std dev	10.2	5.1	4.4	3.3	4.0
pK_a est ave	−7.6	−8.8	−12.3	−4.9	−11.6
pK_a est std dev	11.0	4.7	4.6	3.7	3.3

[a]Calculated at the DLPNO-CCSD(T)/def2-QZVPP/SMD-DMSO//B3LYP/6-31+G(d)/SMD-DMSO level of theory.

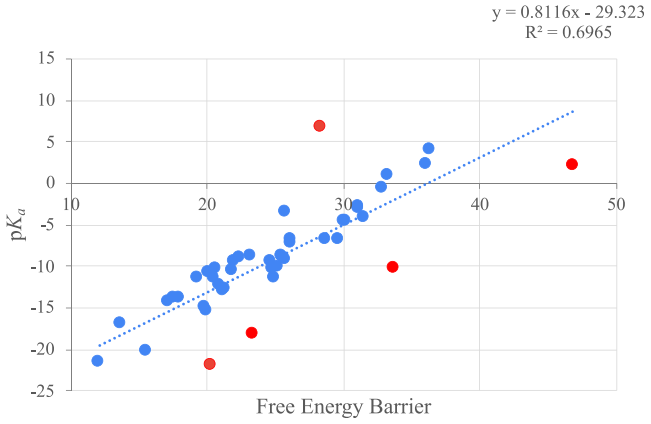

Figure 7. Relationship between free energy barrier and pK_a(C−H) is illustrated using a linear regression indicating that a 1 kcal/mol increase in the free energy barrier corresponds with a ca. 0.8 unit increase in pK_a. Five outliers (red) include AlH_3−Cu^{I}, BH_3−Cu^{I}, AlH_3−Mn^{I}, and PH_3−Mn^{I} below the line of best fit and H_2O−Mn^{I} above the line of best fit. Excluding the outliers, the R^2 is 0.81.

Table 5 displays the Lewis acidity for each ligand using the GEI (global electrophilicity index) as a metric. The results indicated that BH_3 was the most Lewis acidic while NH_3 and H_2O were the most Lewis basic. Figure 8 depicts the relationship between GEI and the average Gibbs free energy barrier for each ligand. A good correlation (R^2 = 0.76) was found. Hence, the results suggest that an increased Lewis acidity of the supporting ligand corresponds with a lower free energy barrier for methane activation, providing further support to the relationship shown in Figure 7 between acidity (pK_a(C−H)) and activation barrier.

Table 5. GEI (Global Electrophilicity Index) in eV for Each Ligand Investigated in This Study

	AlH_3	BH_3	HNC	CO	HCN	NH_3	H_2O	PH_3	SH_2
GEI (eV)	1.8	2.0	1.2	1.8	1.2	0.7	0.7	0.9	0.9

Table 3. Average and Standard Deviations of Calculated Properties (Free Energy Barriers (kcal/mol) and pK_a (pK_a Units)) of Ligand−3d Metal Adducts for Each Ligand[a]

	AlH_3	BH_3	HNC	CO	HCN	NH_3	H_2O	PH_3	SH_2
$\Delta G^{\ddagger}$, ave	21.8	21.9	23.2	19.2	22.7	31.5	27.2	30.0	27.5
$\Delta G^{\ddagger}$, std dev	6.2	7.4	4.0	4.4	4.7	5.1	3.7	10.2	4.1
pK_a est, ave	−15.6	−13.7	−9.7	−13.4	−10.9	−1.7	−4.9	−6.1	−5.3
pK_a est, st dev	7.0	4.1	3.2	3.0	4.7	5.1	7.2	5.2	4.4

[a]Calculated at the DLPNO-CCSD(T)/def2-QZVPP/SMD-DMSO//B3LYP/6-31+G(d)/SMD-DMSO level of theory.

https://dx.doi.org/10.1021/acs.jpca.0c04756
J. Phys. Chem. A 2020, 124, 7283−7289

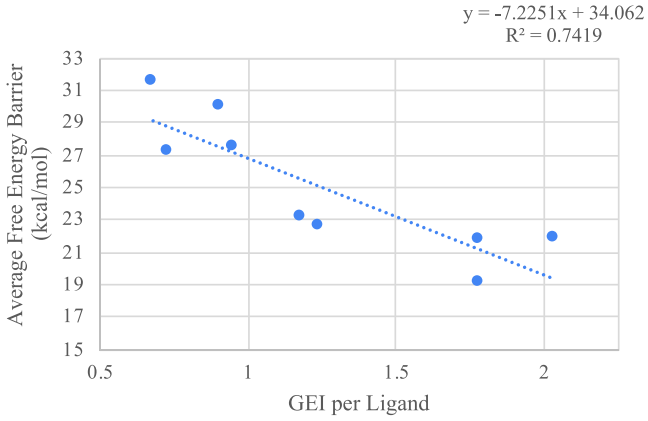

Figure 8. Relationship between GEI and free energy barrier is illustrated using a linear regression (R^2 = 0.74), indicating that increasing Lewis acidity of the ligand corresponds with a decrease in the free energy barrier.

Figures 9−11 depict the geometries of the BH_3−Cu^I methane complexes whose values are an outlier in the graph of the relationship between free energy barrier and pK_a, Figure 7. A single geometry was found for the BH_3−Cu^I methane adduct, Figure 8, but two isomers were found for the transition state, Figure 9, and the BH_3−Cu^I methyl conjugate base, Figure 10. The BH_3−Cu^I conjugate base is interesting in that it involves a short, covalent B−C bond length (1.63 Å), suggesting this as the product of a subsequent functionalization (C−X bond forming) step in the catalytic cycle after the initial C−H activation of methane. Similar considerations apply to other AlH_3 and BH_3 complexes. As a result, multiple conformations were investigated for the AlH_3 and BH_3 complexes, and the final geometries used in the study were selected on the basis of the stationary points with the lowest free energy values.

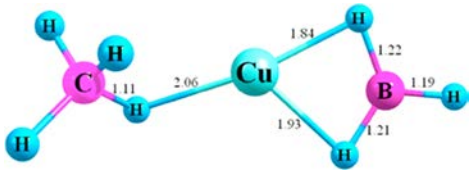

Figure 9. DFT-optimized structure of the BH_3−Cu^I methane adduct.

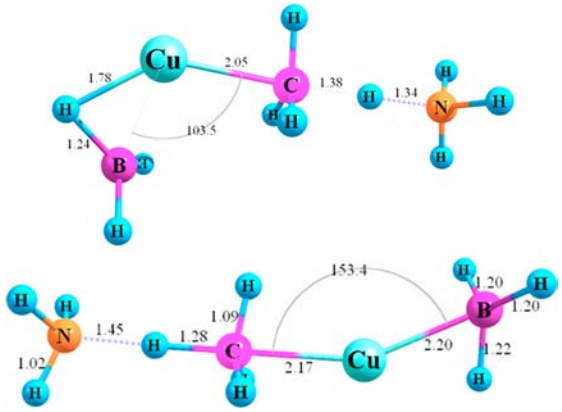

Figure 10. Two isomers were isolated for the BH_3−Cu^I transition state for methane activation by ammonia. The more stable isomer (top) exhibits a bent geometry with a 103.5 °C−Cu−B bond and an activation barrier of 33.7 kcal/mol. The less stable isomer (bottom) has a more linear geometry with a 153.5 °C−Cu−B bond and an activation barrier of 42.7 kcal/mol.

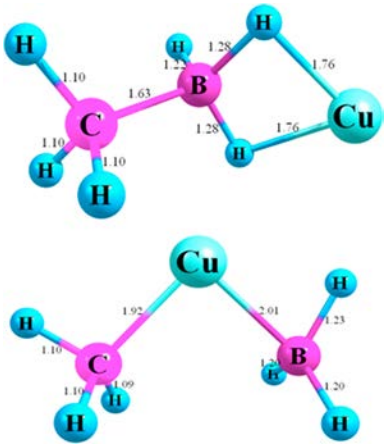

Figure 11. Two isomers of the BH_3−Cu^I methyl complex that were identified by DFT optimization. The more stable isomer (top) is that resulting from a later stage (functionalization) of the reaction with a covalent B−C bond with a free energy change of −2.7 kcal/mol and a pK_a of −27.0. In the less stable isomer (bottom), the borane and the methyl group are both coordinated to Cu without formation of a B−C bond (distance ∼ 2.7 Å) with a free energy change of 2.7 kcal/mol and a pK_a(C−H) of −10.1.

Figure 12 depicts the C−H activation transition state geometries for H_2O−Mn^I models, whose values are an outlier in the graph of the relationship between free energy barrier and pK_a, Figure 7. The transition states exhibited different coordinations between ligand and metal, which likely contributed to contrasting predictions of lowest energy spin state between the B3LYP/6-31+G(d)/SMD-DMSO calculation (predicted a quintet spin state) and DLPNO-CCSD(T)/def2-QZVPP/SMD-DMSO (predicted a septet spin state).

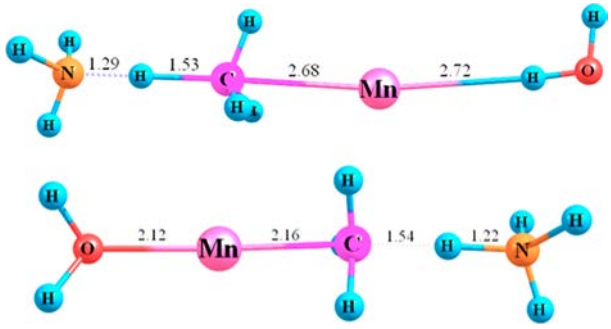

Figure 12. Septet (top) and quintet (bottom) geometries of the H_2O−Mn^I transition state for methane activation by ammonia. B3LYP/6-31+G(d)/SMD-DMSO calculations predicted the septet TS to be more stable, being lower in energy by ∼12.0 kcal/mol. By contrast, single-point calculations at the DFT-optimized geometry with the DLPNO-CCSD(T)/def2-QZVPP/SMD-DMSO technique indicated that the quintet TS is the most energetically favorable structure, ∼12.2 kcal/mol lower in energy. The binding of H_2O in the septet TS occurs through outer sphere binding while the binding mode for the quintet TS occurs through the inner coordination sphere. The largest PNO amplitudes were <0.1 for the septet TS and ∼0.14 for the quintet TS.

SUMMARY AND CONCLUSIONS

The goal of this research was to examine how the combination of supporting ligands and metal identity in simple organometallic

https://dx.doi.org/10.1021/acs.jpca.0c04756
J. Phys. Chem. A 2020, 124, 7283−7289

complexes can impact the acidity of a coordinated methane C−H bond. Both density functional theory, for geometry optimization, and highly accurate DLPNO-CCSD(T)/def2-QZVPP/SMD-DMSO simulations were employed for energetics calculations. The present research indicates that both the supporting ligand *and* the identity of the metal have a significant impact on the pK_a, with coordinated methane pK_a values ranging from −21.8 (AlH_3−Mn^I) to 6.8 (H_2O−Mn^I), a remarkable difference of 28.6 pK_a units, Table 2. Furthermore, the metal and ligand identity also have a significant impact on the activation barrier with a 34.8 kcal/mol difference between the lowest and highest values (12.1−46.9 kcal/mol for AlH_3−Co^I and PH_3−Mn^I, respectively), Table 1. Most importantly, a direct relationship between the pK_a of coordinated methane and the free energy activation barrier was established, Figure 7; specifically, enhancement of the Brønsted acidity of a methane C−H bond upon coordination to the L−M^+ complex was found to correlate with lower barriers to activation of methane.

Certain metals and ligands were clearly more favorable than others in enhancing methane activation. The study indicated that the $[Co{-}AlH_3]^+$ complex had the highest catalytic potential due to its low activation barrier of 12.1 kcal/mol and high acidity of ligated methane at −21.6 pK_a units, Tables 1 and 2. Interestingly, barriers tended to be lower for ligands that were Lewis acids such as AlH_3 and BH_3 as well as π-acids such as CO and HNC, Table 3. In light of the correlation between the lower pK_a of the ligated methane and the lower free energy barrier of methane activation, Figure 7, it is hypothesized that such ligands yield a more electron deficient metal, which in turn enhances the acidity of the ligated methane C−H bonds. This hypothesis is further reinforced by the strong correlation found between Lewis acidity of the supporting ligand and the Gibbs free energy barrier for methane activation, Figure 8. Moreover, one may argue that Z-type ligands deserve additional experimental scrutiny as supporting ligands for methane functionalization catalysis.

While both metals and ligands tested in this study affected the acidity of coordinated methane and hence the kinetic favorability of the subsequent methane activation reaction, ligands displayed a slightly wider range of variation, Tables 3 and 4. The highest and lowest average ligand $\Delta G^{\ddagger}$ differed by 12.3 kcal/mol from 19.2 kcal/mol (CO) to 31.5 kcal/mol (NH_3), Table 3. This can be compared to the 10.4 kcal/mol difference in $\Delta G^{\ddagger}$ between the extreme averages for the metals modeled, which ranged from 19.5 kcal/mol (Co^I) to 29.9 kcal/mol (Ni^I), Table 4.

Analysis of the individual impacts of the ligands and metals also revealed promising results. Among all metals investigated, LCo^I complexes were found to have the lowest free energy barriers, with an average of 19.5 ± 4.4 kcal/mol, which indicates that the cobalt complexes are the most energetically favorable among the models studied for methane activation, Table 4. The pK_a values corresponding to the cobalt complexes were the most acidic overall, with an average pK_a of −12.3 pK_a units, Table 4. Thus, the cobalt complexes again illustrate the strong positive correlation observed between increased acidity of the coordinated methane C−H bonds and lowered kinetic activation barriers, Figure 7.

Among the studied ligands, CO yielded the lowest free energy barrier of 19.2 kcal/mol along with one of the lowest pK_a values of −13.4 units, Table 3. In a similar vein, AlH_3 complexes were shown to have the lowest pK_a of all metal−ligand pairs, with an average pK_a of −15.6 pK_a units, as well as the second lowest free energy barrier among the ligands studied, with an average of 21.8 kcal/mol, Table 3. However, there were two exceptions to this correlation between pK_a and activation barrier concerning AlH_3: the AlH_3−Cu^I and AlH_3−Mn^I complexes. As discussed above, group 13/Cu^I, as well as several Mn^I complexes, were found to be outliers in the methane pK_a vs $\Delta G^{\ddagger}$ correlation (Figure 7, data points highlighted in red), implying that additional factors other than the acidity of the coordinated methane may determine the actual activation barrier. Some potential factors include the thermodynamic stability of the intermediate generated by methane activation, metal spin state, and the location of the supporting ligand in either the inner or outer coordination sphere of the metal.

In future studies, solvents other than DMSO could also be modeled. Another area of future interest is the testing of additional ligands. In this study, only nine simple ligands were probed for thermodynamic relationships in methane deprotonation. To test the theory derived from this study, more complex ligands with properties similar to the promising Z-type ligands such AlH_3 and BH_3 and π-acids such as CO and HNC could be investigated to create more industrially practical catalyst leads. Finally, future work should focus on the impact of the metal's formal oxidation state on methane activation barriers. This has been indicated to be a promising avenue for future research given the correlation between methane acidity and methane activation barriers and is currently under investigation in our group.

■ ASSOCIATED CONTENT

Supporting Information

The Supporting Information is available free of charge at https://pubs.acs.org/doi/10.1021/acs.jpca.0c04756.

Predicted ground states of ligand−3d metal methane adducts, spin state trend analyses, and data on the free energy change values (kcal/mol) of the complexes (PDF)

Cartesian coordinates for the B3LYP/6-31+G(d)/SMD-DMSO-optimized geometries for which the CCSD(T)/def2-QZVPP/SMD-DMSO single-point energies were calculated (XYZ)

■ AUTHOR INFORMATION

Corresponding Author

Thomas R. Cundari − *Department of Chemistry Center for Advanced Scientific Computing and Modeling (CASCaM), University of North Texas, Denton, Texas 76203-5070, United States;* orcid.org/0000-0003-1822-6473; Email: t@unt.edu

Authors

Amy S. Guan − *Department of Chemistry Center for Advanced Scientific Computing and Modeling (CASCaM), University of North Texas, Denton, Texas 76203-5070, United States;* orcid.org/0000-0002-6230-9818

Ivy X. Liang − *Department of Chemistry Center for Advanced Scientific Computing and Modeling (CASCaM), University of North Texas, Denton, Texas 76203-5070, United States*

Christopher X. Zhou − *Department of Chemistry Center for Advanced Scientific Computing and Modeling (CASCaM), University of North Texas, Denton, Texas 76203-5070, United States;* orcid.org/0000-0002-7839-0817

Complete contact information is available at: https://pubs.acs.org/10.1021/acs.jpca.0c04756

Notes

The authors declare no competing financial interest.

■ ACKNOWLEDGMENTS

The authors thank the National Science Foundation for their generous support through Grants CHE-1464943 and CHE-1953547, and their support of the UNT CASCaM HPC cluster via Grant CHE-1531468.

■ REFERENCES

(1) Gunsalus, N. J.; Koppaka, A.; Park, S. H.; Bischof, S. M.; Hashiguchi, B. G.; Periana, R. A. Homogeneous Functionalization of Methane. *Chem. Rev.* **2017**, *117* (13), 8521−8573.
(2) Shilov, A. E.; Shul'pin, G. B. Activation of C−H Bonds by Metal Complexes. *Chem. Rev.* **1997**, *97* (8), 2879−2932.
(3) Hu, A.; Guo, J.-J.; Pan, H.; Zuo, Z. Selective Functionalization of Methane, Ethane, and Higher Alkanes by Cerium Photocatalysis. *Science* **2018**, *361* (6403), 668−672.
(4) Olah, G. A.; Schlosberg, R. H. Chemistry in Super Acids. I. Hydrogen Exchange and Polycondensation of Methane and Alkanes in FSO_3H-SbF_5 ("Magic Acid") Solution. Protonation of Alkanes and the Intermediacy of CH_5 and Related Hydrocarbon Ions. The High Chemical Reactivity of "Paraffins" in Ionic Solution Reactions. *J. Am. Chem. Soc.* **1968**, *90*, 2726−2727.
(5) Streitwieser, A.; Taylor, D. R. Kinetic Acidity of Methane. *J. Chem. Soc. D* **1970**, No. 19, 1248.
(6) Caballero, A.; Despagnet-Ayoub, E.; Mar Diaz-Requejo, M.; Diaz-Rodriguez, A.; Gonzalez-Nunez, M. E.; Mello, R.; Munoz, B. K.; Ojo, W.-S.; Asensio, G.; Etienne, M.; Perez, P. J. Silver-Catalyzed C-C Bond Formation Between Methane and Ethyl Diazoacetate in Supercritical CO2. *Science* **2011**, *332*, 835−838.
(7) Pitsawong, W.; Chenprakhon, P.; Dhammaraj, T.; Medhanavyn, D.; Sucharitakul, J.; Tongsook, C.; van Berkel, W. J. H.; Chaiyen, P.; Miller, A.-F. Tuning of pKa Values Activates Substrates in Flavin-Dependent Aromatic Hydroxylases. *J. Biol. Chem.* **2020**, *295* (12), 3965−3981.
(8) Zhou, C. X.; Cundari, T. R. Computational Study of 3d Metals and Their Influence on the Acidity of Methane C−H Bonds. *ACS Omega* **2019**, *4* (23), 20159−20163.
(9) Ho, J.; Coote, M. L. PKa Calculation of Some Biologically Important Carbon Acids - An Assessment of Contemporary Theoretical Procedures. *J. Chem. Theory Comput.* **2009**, *5* (2), 295−306.
(10) Christman, W. E.; Morrow, T. J.; Arulsamy, N.; Hulley, E. B. Absolute Estimates of $Pd^{II}(h^2$-Arene) C−H Acidity. *Organometallics* **2018**, *37* (16), 2706−2715.
(11) Frisch, M. J.; Trucks, G. W.; Schlegel, H. B.; Scuseria, G. E.; Robb, M. A.; Cheeseman, J. R.; Scalmani, G.; Barone, V.; Petersson, G. A.; Nakatsuji, H.; et al. *Gaussian 16, Revision A.03*; Gaussian, Inc.: Wallingford, CT, 2016.
(12) Neese, F. The ORCA Program System. *Wiley Interdiscip. Rev.: Comput. Mol. Sci.* **2012**, *2*, 73−78.
(13) Neese, F. Software Update: The ORCA Program System, Version 4.0. *Wiley Interdiscip. Rev.: Comput. Mol. Sci.* **2018**, *8* (1), e1327.
(14) Nazemi, A.; Cundari, T. R. Control of C−H Bond Activation by Mo-Oxo Complexes: PKa or Bond Dissociation Free Energy (BDFE)? *Inorg. Chem.* **2017**, *56* (20), 12319−12327.
(15) Jupp, A. R.; Johnstone, T. C.; Stephan, D. W. The Global Electrophilicity Index as a Metric for Lewis Acidity. *Dalton Trans.* **2018**, *47* (20), 7029−7035.

https://dx.doi.org/10.1021/acs.jpca.0c04756
J. Phys. Chem. A 2020, 124, 7283−7289